Numerical solution of reinforced concrete beam using Newton-Raphson method with adaptive descent

PIOTR SMARZEWSKI

Lublin University of Technology, Faculty of Civil Engineering and Architecture,
40 Nadbystrzycka St., 20-618 Lublin, Poland, p.smarzewski@pollub.pl

Abstract. This paper describes numerical solution of a reinforced concrete beam. The modelling was performed with the principles of the Finite Element Method (FEM). In order to validate the materials models: concrete and reinforcing steel, the results, obtained using the Newton-Raphson method with adaptive descent, were compared with experimental data. Simulations help to reduce the cost of experimental research through more efficient carrying out the tests. The solution of advanced problems of reinforced concrete members in the range of linear-elastic deformation and in the range of non-linear deformation leading to the failure is possible.
Keywords: mechanics of concrete structures, finite element method, reinforced concrete beam, adaptive descent

1. Introduction

FEM software allows for the analysis of advanced computational problems of building structures such as simulating environmental impacts, non-linear buckling analysis, and work of reinforced concrete structures. Modern approach to the numerical analysis requires the formation of three-dimensional models taking into account the non-linear properties.

On the basis of the FEM and the finite difference method (FDM), the mesh free method (MFree), the extended finite element method (XFEM), and the numerical manifold method (NMM) are developed. These methods are numerical techniques based on the generalized finite element method (GFEM) and the partition of unity method (PUM). They extend the classical methods approach by enriching the solution

space for solutions to differential equations with discontinuous functions. All these methods have advantage over conventional mesh-based approaches in dealing with problems involving large deformation and crack propagation [1]. XFEM procedures used in the simulation of crack propagation and contact detection were made available in the ABAQUS system. These problems are described in several studies [2-4].

The subject of the paper is a reinforced concrete beam composed of concrete and steel rebars arranged discretely modelled using ANSYS.

The aim of this paper is to model the mechanisms of failure in the reinforced concrete beam under static load, with physical non-linearity of materials: concrete and reinforcing steel. Concrete model for elastic-plastic material with the consideration for softening in compression and tension was applied. The original analyses for spatial reinforced concrete beam in the range of large displacement static were made. According to Eurocode 2, the method of nonlinear analysis concerning geometrical non-linearity can be used with non-linearity in a physical sense within the 2nd class theory [5].

Numerical analyses of C1-reinforced concrete beam, tested by Buckhouse [6], were carried out. The solution of the incremental equations of static equilibrium in FEM was conducted using Newton-Raphson method with adaptive descent.

2. Modelling of materials

2.1.   Modelling of concrete

The failure surface was presented with a five-parameter concrete model [7]. The failure criterion in a complex state of stress is described as follow:

$$\frac{F}{f_c} - S \geq 0, \tag{1}$$

in which: F — the function of stresses conditions σ_{xp}, σ_{yp}, σ_{zp} in the direction of the Cartesian coordinate system xyz; S — failure surface dependent on the principal stresses σ_1, σ_2, σ_3, where $\sigma_1 = \max(\sigma_{xp}, \sigma_{yp}, \sigma_{zp})$; $\sigma_3 = \min(\sigma_{xp}, \sigma_{yp}, \sigma_{zp})$ and $\sigma_1 \geq \sigma_2 \geq \sigma_3$ and five strength parameters. More information about the function of stresses and failure surface was presented in [8].

Figure 1 shows the failure surface in biaxial stress state transformed to σ_{xp}-σ_{yp} surface in the area of the highest non-zero normal stresses σ_{xp}, σ_{yp}. The states of material safe work are located inside the surface which evolution is represented by material hardening or softening.
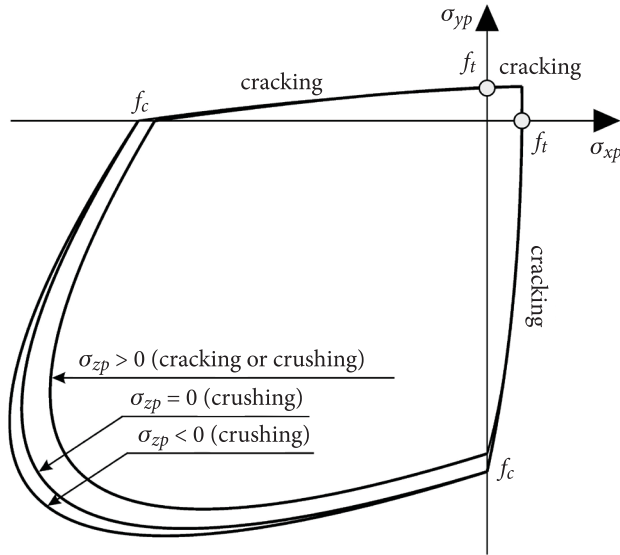
Fig. 1. Failure surface

The equations for the stress-strain curve are useful in the structure analysis. Numerical solutions of reinforced concrete beams according to the equations given in [9] were characterized by lower ultimate deflection.

The idea of concrete behaviour in the uniaxial compression and tension is proposed (see Fig. 2). The stress-strain relation for the concrete is the combination of Desayi-Krishnan [10] and Stolarski [11] propositions. The elastic-plastic hardening in the uniaxial compression, the material softening and the test ultimate strains of Pecce, Fabbrocino [12], and Kamińska [13] were included.
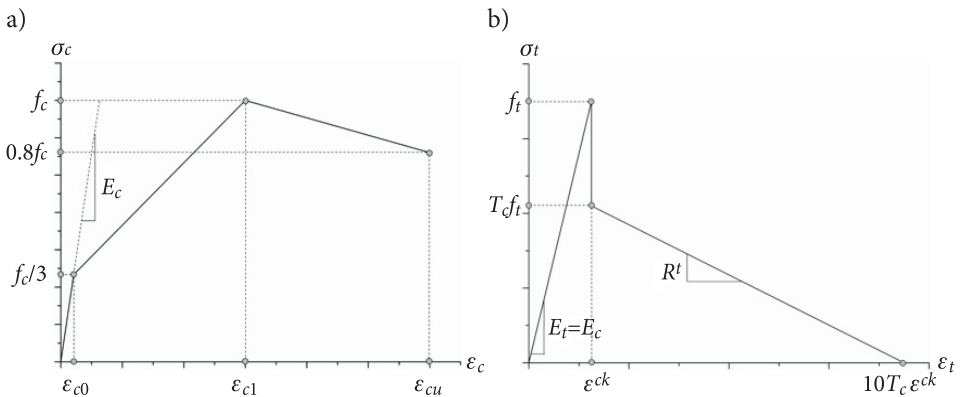

Fig. 2. Stress-strain relation for concrete in uniaxial: a) compression; b) tension

The elastic behaviour of concrete in compression is dependent on the reinforcement amount and concrete strength. Linear function is assumed for the concrete compression to 33% of the ultimate uniaxial compressive strength (f_c). Then concrete is worked in the phase of elastic-plastic with hardening up to f_c. After reaching f_c concrete is softened to $0.8f_c$ at ultimate strain ε_{cu}.

In the studies, conducted by Kamińska [13], some beams were damaged by the concrete crushing. Strains reached 6‰ and they were two times higher than the ultimate strains measured on the samples. For this reason, the larger compressive strain is adopted in the numerical analysis. The concrete compressive strain ε_{c1} at f_c is 6‰ whereas the ultimate compressive strain ε_{cu} is 12‰.

The stress-strain relation in tension for the concrete is linear to the uniaxial tensile strength (f_t). On the basis of Lyndon and Balendran [14], equal modulus of elasticity in compression and tension are assumed. After reaching f_t, crack appears and brittle fracture occurs to the value equal or higher than $0.6f_t$. T_c parameter should be selected from $0.6 \leq T_c \leq 1$. This stiffening effect is a gradual, smooth descent of f_t to zero. Concrete strains is 0.8‰, $T_c = 0.6$, and 1.4‰, $T_c = 1$.

2.2. Modelling of steel

Steel in a form of reinforcing bars is used in concrete structures. This reduces the problem of modelling of steel to the state of uniaxial stress. Model of elastic-plastic material for the reinforcing steel with identical properties at compressive and tensile is applied. Linear-elastic model for the steel plates located in the support area and at the load point is assumed. Figure 3 presents the stress-strain relation for the reinforcing steel.
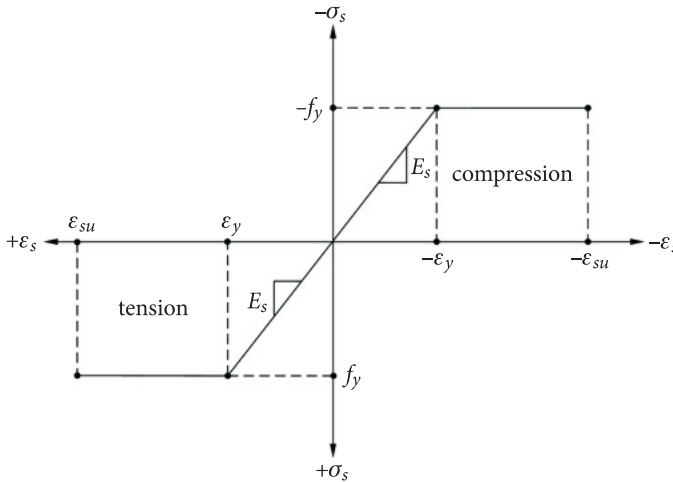

Fig. 3. Stress-strain relation for reinforcing steel

3. Method of analysis

3.1. Modelling of reinforced concrete beam

Model of the reinforced concrete beam corresponds to C1-beam tested by Buckhouse [6]. The dimensions, the reinforcement arrangement, and the load scheme are presented in Fig. 4.
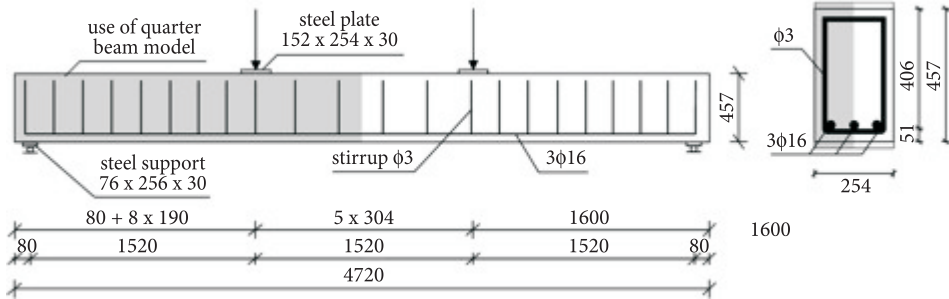

Fig. 4. Dimensions, reinforcement arrangement, and load scheme of reinforced concrete beam
(unit in mm) [6]

The model of concrete is defined by the following parameters: uniaxial compressive strength f_c = 33.1 MPa (tested by [6]), modulus of elasticity $E_c = 57000 f_c^{1/2}$ = 27228.1 MPa (according to ACI 318, f_c [pound/inch^2], [15]), uniaxial tension strength $f_t = 7.5 f_c^{1/2}$ = 3.6 MPa (f_c [pound/inch^2], [15]), Poisson ratio v_c = 0.2, ultimate strain in elastic-plastic hardening area ε_{c1} = 6‰, ultimate strain in softening area ε_{cu} = 12‰, shear transfer coefficients for an open crack β_t = 0.5 (estimated on the basis of Bangash [16], Hemmaty et al. [17, 18], Kachlakev et al. [19], Waszczyszyn [20], Wolanski [21] and Smarzewski [22]), shear transfer coefficients for a closed crack β_c = 0.99.

The model of reinforcing steel and the model of supporting plates are defined by the following parameters: modulus of elasticity E_s = 200 GPa, yield stress f_y = 413.7 MPa, tensile strength f_{st} = 550 MPa, Poisson ratio v_s = 0.3, and cross-sectional area of reinforcement A_{s1} = 6.03 cm^2.

Due to the symmetry in cross-section of the concrete beam and loading, only one quarter of the beam is modelled. The length, width, and height of the beam are 2360 mm, 127 mm, and 457 mm, respectively. Figure 5 presents the FE mesh for the C1 beam model, support and loading plate. The FE dimensions are given in the following order: length, width, and height. No mesh of the reinforcement is needed because elements are created in the modelling through the nodes created by the mesh of the concrete volume.
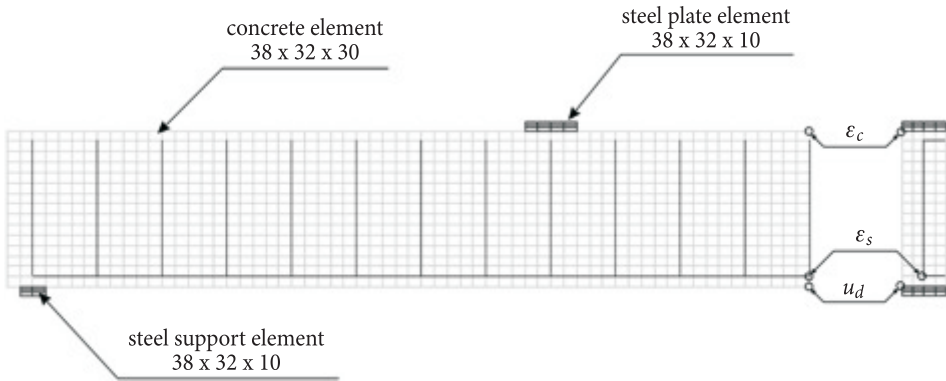
Fig. 5. Mesh of one quarter C1-beam model with marked control locations of displacement and strain (unit in mm)

An important step in FEM is the selection of the mesh density. A convergence of results is obtained when an adequate number of elements is used in a model. This is practically achieved when an increase in the mesh density has a negligible effect on the results. The 3720 element model, which was equivalent to 14880 elements in the full-beam model, was selected for the C1-beam model. The results started to converge with a model having approximately 12000 elements for the entire beam.

3.2. FE modelling of steel reinforcement

The discrete model for modelling of steel reinforcement in FEM for reinforced concrete beam is applied. In this study, perfect bond between materials is assumed.
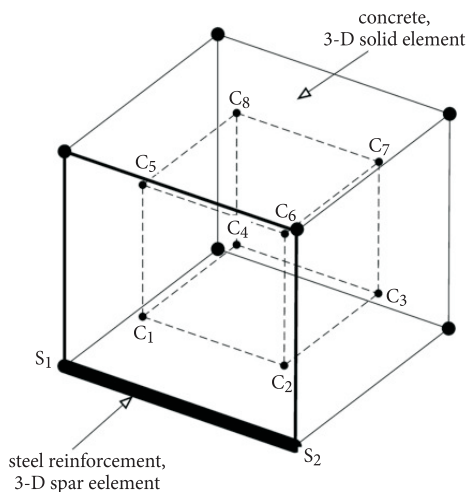

Fig. 6. Discrete model for reinforcement in reinforced concrete beam

To provide the perfect bond, the reinforcement in the discrete model uses 3-D spar elements that are connected to concrete mesh nodes (Fig. 6). Consequently, the concrete and the reinforcement mesh share the same nodes and concrete occupies the same regions seized by reinforcement. A disadvantage to this model is that the concrete mesh is restricted by the location of the reinforcement and the volume of the steel reinforcement is not removed from the concrete volume. 3-D spar elements are used to create the flexural and the shear reinforcement. The tensile bars share the same nodes at the points that they intersect the shear stirrups.

3.3. Boundary conditions and loads

Displacement boundary conditions are needed to constrain the beam model. Boundary conditions are applied at the points of symmetry, and at the supports and loadings exist to ensure the model acting in the same way as the tested beam.

The symmetry boundary conditions are set. The beam model being used is symmetric about two planes. The support plate is modelled as a roller allowing one to rotate the beam along the plane xy. A single line of nodes on the plate are given constraints in $u_x = 0$ and $u_z = 0$ directions. The force F is applied across the entire centreline at each node on the steel plate. The boundary conditions for support and at the loading plate are illustrated in Fig. 7.
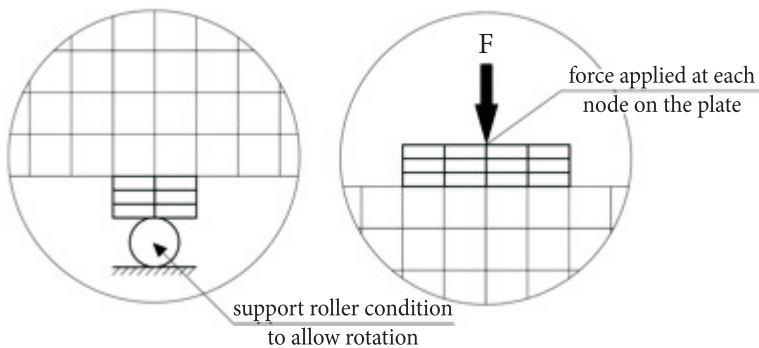

Fig. 7. Boundary conditions at support and loading plates

3.4. Newton-Raphson method with adaptive descent

Adaptive descent method studied by Eggert et al. [23] is based on the change of solution path approximating the limit point and reversing along the secant until obtaining the convergence of numerical solution. The stiffness matrix is written as:

$$[K_i^T]\{\Delta u_i\} = \{F^a\} - \{F_i^{nr}\}, \tag{2}$$

where: $[K_i^T]$ — tangent stiffness matrix;

i — index corresponding to the number of the incremental step;

$\{F_i^{nr}\}$ — vector of restoring loads representing the element internal loads in the discretised system.

It is described as a sum of two matrixes:

$$[K_i^T] = \xi[K^S] + (1-\xi)[K^T], \tag{3}$$

$[K^S]$ — secant stiffness matrix;

$[K^T]$ — tangent stiffness matrix;

ξ — adaptive descent parameter.

The method requires defining the adaptive descent parameter ξ during iteration of equilibrium:

1. At the beginning of each substep tangent stiffness matrix is calculated according to Newton-Raphson's method, with the consideration for adaptive descent parameter $\xi = 0$ in Eq. (3).

2. For subsequent iterations of equilibrium, the variability of the solution $||\{R\}||_2 = (\Sigma\, R_i^2)^{1/2}$ is monitored, for the unbalanced load vector $\{R\}=\{F^a\}$ — $\{F^{nr}\}$ — the right side of Eq. (2).

When the norm grows, the disconvergence of the solution is probable. When it falls, the convergence of solution is possible. The adaptive descent parameter ξ is balanced while making iteration until the required convergence of the numerical solution is reached. The secant stiffness matrix is generated as a result of solving non-linear tasks concerning plasticity, structure stiffness with large displacements or concrete crushing.

In this study, for the reinforced concrete solid elements, convergence criteria were based on displacement. It was found that convergence of solutions was difficult to achieve due to the non-linear behaviour of reinforced concrete. Therefore, the convergence tolerance limits were increased to a maximum of 5 times the default tolerance limits of 5% for displacement checking in order to obtain convergence of the solutions.

4. Numerical results and discussion

4.1. Cracking analysis

Figure 8 shows the development of the tensile force in the steel. In the smeared cracking approach, the smeared cracks spread over the region where the principal

tensile stresses in the concrete elements exceed the ultimate tensile strength (see Fig. 8a, 8b). The stiffness of the cracked concrete elements in the FE model reduces to zero, so they cannot resist tension. Therefore, the tension in the steel FE does not vary as in the actual beam. The tensile force in a steel element is constant across the element (see Fig. 8c). For this reason, FEA-strains could be higher than the measured strains. This could also explain the difference in the steel yielding loads between the FE model and the experimental results.
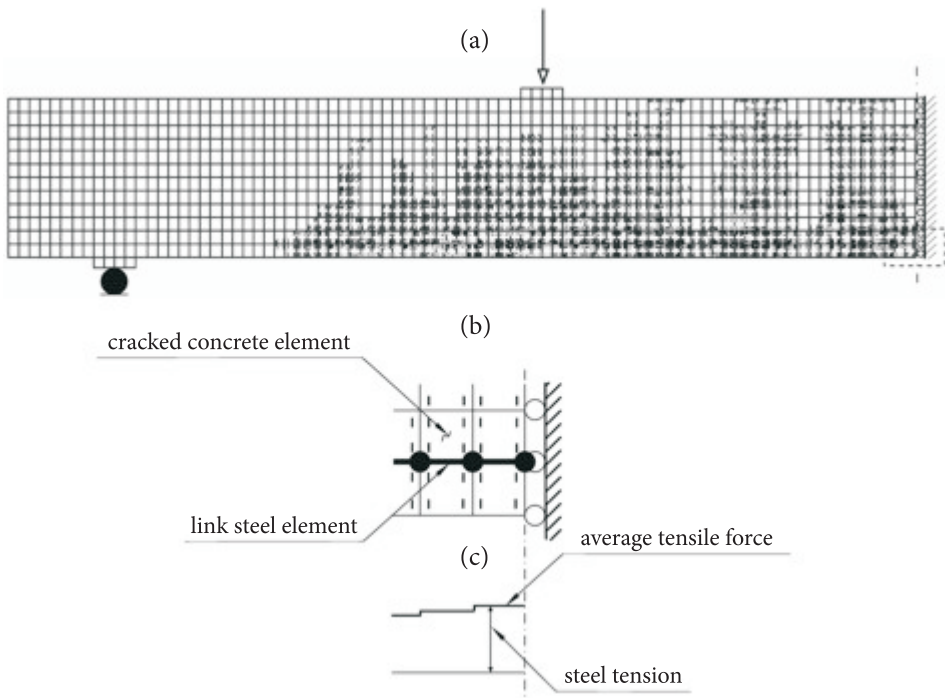

Fig. 8. Development of tensile force in steel: (a) smeared cracking pattern; (b) cracked concrete and steel rebar element; (c) tensile force in steel elements

Figure 9 presents the smeared crack patterns obtained at different load. Flexural cracks increases in the constant moment region, up to 31 kN, and the beam begins cracking out towards the support plate. Significant flexural cracking occurs in the beam at 57.8 kN. Diagonal cracks are beginning to form in the model shear-span after reinforcement yielding at 64 kN. More cracks have now formed in the constant moment region. Cracking has reached the top of the beam.

At load 70.9 kN, the model beam no longer can support additional load as indicated by convergence failure. In the test [6], control beam failed at load 72.6 kN. The ultimate load of the FE model beam was within 3% of the ultimate load of the control beam.
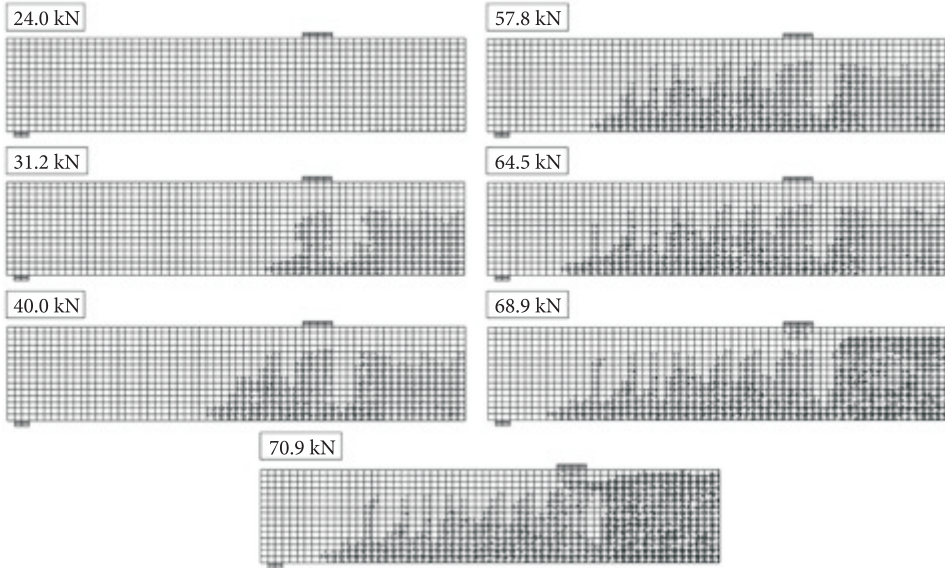
Fig. 9. Smeared crack patterns

4.2.   Strain and stress analysis

The FEA compressive strain data for concrete are collected from the point placed on the top face of the beam as shown in Fig. 5. The tensile strain data for main steel reinforcement are collected on the φ16 mm steel rebar at mid-span (see Fig. 5). Figure 10a presents the load-compressive strain curve for the concrete from the FEA in the C1-beam. Figure 10b shows the load-tensile strain plot for the main steel reinforcing at mid-span from the FEA in the C1-beam.
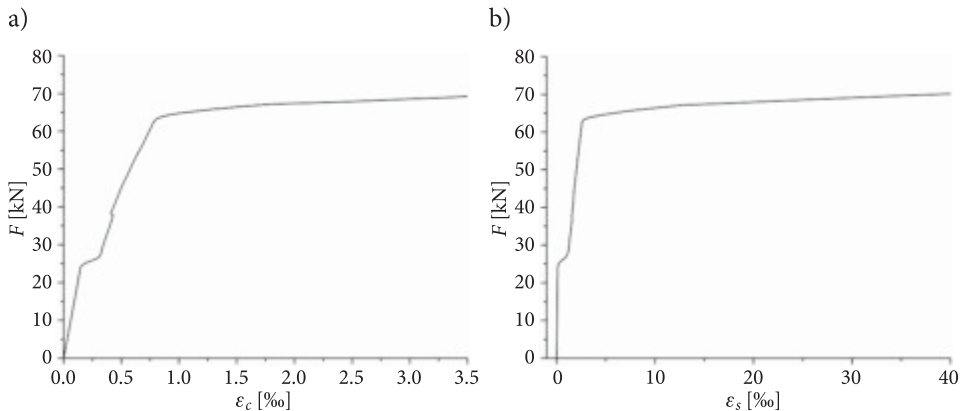
a)   b)

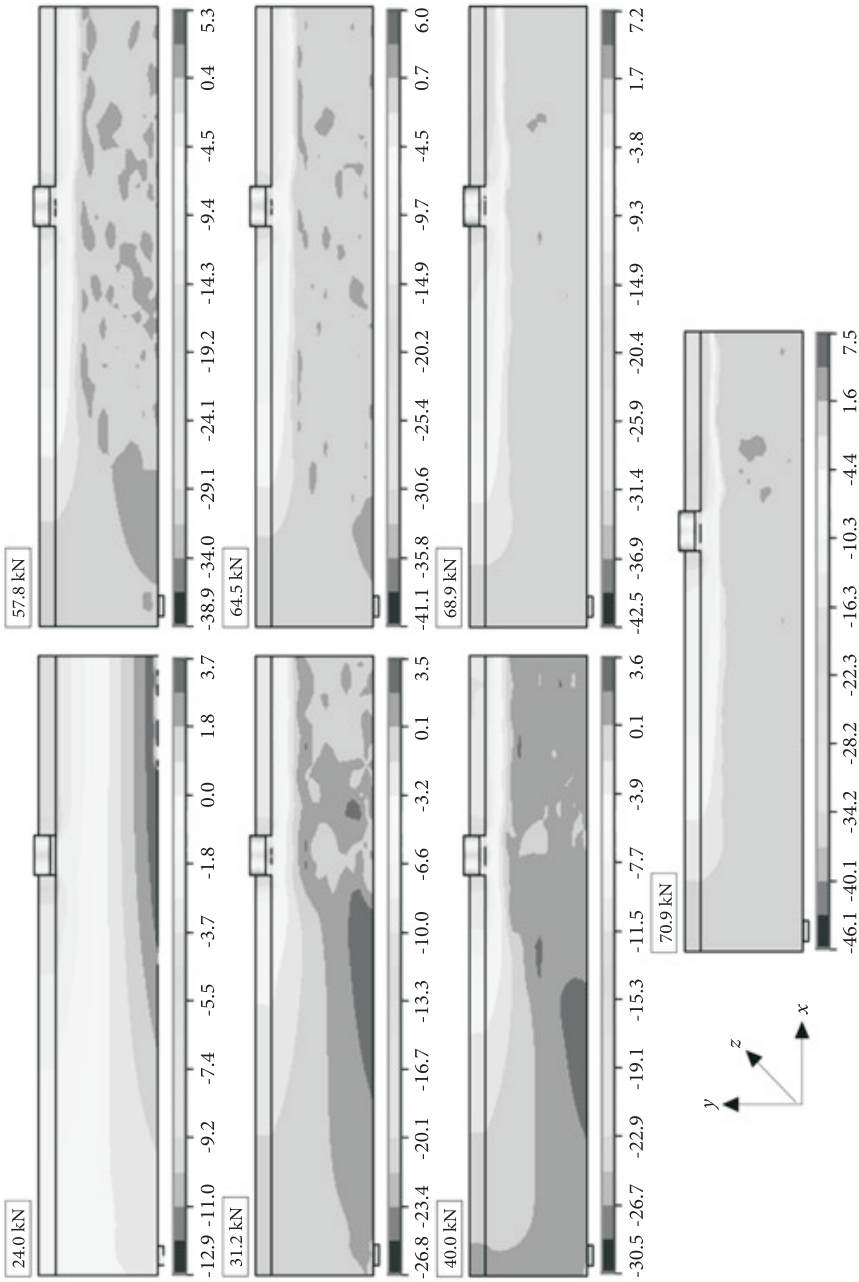Fig. 10. Load-strain curves for: a) compressive concrete; b) tensile main steel rebar

Fig. 11. Normal stresses σ_x (unit in MPa)

Figure 11 shows the development of normal stresses σ_x for the left quarter of the model beam. The evolutions of stresses are presented by beam rotation of 20° around the x-axis, in order to show their changes in the top face of the beam.

Under the load $F = 24$ kN, the development of stress corresponding to the elastic behaviour of the beam is observed. For this load one can observe a tension in concrete below the neutral axis in the plasticity area. Its influence on the total load capacity is insignificant and frequently neglected in calculations, especially at high cross-sectional area of reinforcement. Yet, for a low cross-sectional area of reinforcement, its influence is slightly higher, however, it is neglected due to the possibility of occurring incidental crack. Below the plasticity area in the constant moment region, one can notice a small cracking area. After the increase in the load to $F = 31.2$ kN, the cracking area and concrete plasticity area increase. Between smeared cracks there are significant discrepancies in stress distribution. With the increase in load, one can observe the approximation of neutral axis to the top face of the beam. At the level of $F = 40$ kN, the increase in the plasticity area can be observed. Neutral axis is the boundary between cracked and un-cracked planes. The increase in neutral axis in the 3rd phase is experimentally proved. At the load of 57.8 kN, one can see the development of stress at the support. For the load of $F = 68.9$ kN, one can observe gradual development of stress upwards. It is also possible to notice further development of compressive concrete plasticity in the constant moment region. For the load of $F = 70.9$ kN, the beam load capacity was reached and the concrete was locally crushed at the top face of the model beam, similarly to tested beam [6].
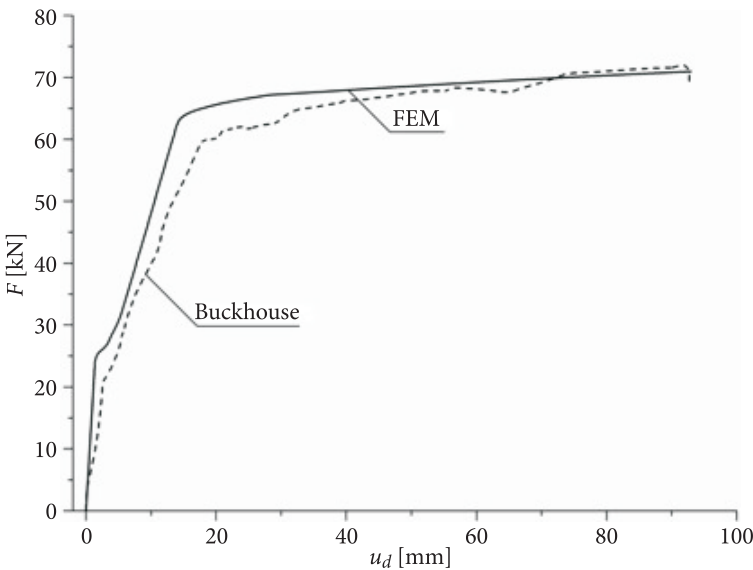

Fig. 12. Load-deflection curves at C1-beam mid-span

4.3.   Load-deflection analysis

Figure 12 illustrates the comparison of the load-deflection curves from the FE analysis with the experimental data at mid-span for C1-beam. In the linear range and after cracking, the load-deflection curve form the FEA is stiffer than that from the test results. The first cracking load for the FEA is higher from the experimental results by 12%. Steel reinforcement yielding is illustrated by a sudden stiffness decrease in the beam on the plot load-deflection. Ultimate deflection at beam mid-span of 93 mm from the model is higher than the experimental ultimate deflection of 92.7 mm by only 0.3%. The FEA agrees well with the experimental data for the C1-beam.

Summary

The paper evaluates the FEM effectiveness for analysing non-linear behaviour of reinforced concrete beam modelled as spatial structural member, without simplifications regarding technical assumptions of a beam theory.

The method of strain analysis was based on the FEM rules. Perfect bond between steel rebars and concrete was assumed. The smeared crack model for concrete and discrete reinforcement was used. The solution was obtained by quasi-Newton numerical method.

On the basis of reinforced concrete beam under static load it was presented a comparison of the FEA with the experimental results. The comparison proved the correctness of the assumptions concerning the concrete model, steel models and numerical analysis to solve non-linear equilibrium equations. The modelling of reinforced concrete beams reflects non-linear response of the flexure members under loading, up to failure. Solving non-linear structural member with the use of Newton-Raphson method with adaptive descent can precisely locate the strain states and can locate the decrease for response curve after steel rebars yielding.

Simulations can contribute to the reduction of research costs by more effective experiment planning and can limit the number of tested samples. They allow for the analysis of complex structure behaviour in the entire deformation range.

REFERENCES

[1]   Liu G.R., *Mesh free methods: moving beyond the Finite Element Method*, CRC Press LLC, 2003.

[2]   Marzec I., Tejchman J., *Enhanced coupled elasto-plastic-damage model to describe cyclic concrete behaviour*, CMM-2011 — Computer Methods in Mechanics, Warsaw, Poland, 9-12 May 2011.

[3] KOROL E., TEJCHMAN J., *Experimental and theoretical studies on size effects in concrete and reinforced concrete beams*, CMM-2011 — Computer Methods in Mechanics, Warsaw, Poland, 9-12 May 2011.

[4] BOBIŃSKI J., TEJCHMAN, *Modeling cracks in concrete elements with XFEM*, CMM-2011 — Computer Methods in Mechanics, Warsaw, Poland, 9-12 May 2011.

[5] PN-EN 1992-1-1: wrzesień 2008, Eurokod 2: *Projektowanie konstrukcji z betonu*. Część 1-1: *Reguły ogólne i reguły dla budynków*.

[6] BUCKHOUSE E.R., *External Flexural Reinforcement of Existing Reinforced Concrete Beams Using Bolted Steel Channels*, Master's Thesis, Marquette University, Milwaukee, Wisconsin, 1997.

[7] WILLAM K.J., WARNKE E.P., *Constitutive Model for the Triaxial Behavior of Concrete*, International Association for Bridge and Structural Engineering, vol. 19, ISMES, Bergamo, Italy, 1975, p. 1-30.

[8] SMARZEWSKI P., STOLARSKI A., *Modelowanie zachowania niesprężystej belki żelbetowej*, Biul. WAT, vol. 56, nr 2, 2007, p. 147-166.

[9] COMITÉ EURO-INTERNATIONAL DU BETON, *High Performance Concrete. Recommended to the Model Code 90. Research Need*, Bulletin d'Information, nr 228, 1995.

[10] DESAYI P., KRISHNAN S., *Equation for the Stress-Strain Curve of Concrete*, Journal of the American Concrete Institute, 61, March 1964, p. 345-350.

[11] STOLARSKI A., *Dynamic Strength Criterion for Concrete*, Journal of Engineering Mechanics, American Society of Civil Engineering, vol. 130, nr 12, December 2004, p. 1428-1435.

[12] PECCE M., FABBROCINO G., *Plastic Rotation Capacity of Beams in Normal and High-Performance Concrete*, ACI Structural Journal, March-April 1999, p. 290-296.

[13] KAMIŃSKA M.E., *Doświadczalne badania żelbetowych elementów prętowych z betonu wysokiej wytrzymałości*, KILiW, PAN, Łódź, 1999.

[14] LYNDON F.D., BALENDRAN R.V., *Some observations on elastic properties of plain concrete*, Cement and Concrete Research, 16, nr 3, 1986, p. 314-324.

[15] ACI 318-99, *Building Code Requirements for Reinforced Concrete*, American Concrete Institute, Farmington Hills, Michigan, 1999.

[16] BANGASH M.Y.H., *Concrete and Concrete Structures: Numerical Modeling and Applications*, Elsevier Science Publishers Ltd., London, England, 1989.

[17] HEMMATY Y., DEROECK G., VANDERWALLE L., *Parametric Study of RC Corner Joints Subjected to Positive Bending Moment by Nonlinear FE Model*, Proceedings of the ANSYS Conference, vol. 2, Pittsburgh, Pennsylvania, June 1992.

[18] HEMMATY Y., *Modelling of the Shear Force Transferred Between Cracks in Reinforced and Fibre Reinforced Concrete Structures*, Proceedings of the ANSYS Conference, vol. 1, Pittsburgh, Pennsylvania, August 1998.

[19] KACHLAKEV D.I., MILLER T., YIM S., CHANSAWAT K., POTSIUK T., *Finite Element Modeling of Reinforced Concrete Structures Strengthened with FRP Laminates*, California Polytechnic State University, et al., May, 2001.

[20] WASZCZYSZYN Z., *Numerical problems of nonlinear stability analysis of elastic structures*, Computers and Structures, 17(1), 1983, p. 13-24.

[21] WOLANSKI B.S., *Flexural Behavior of Reinforced and Prestressed Concrete Beams Using Finite Element Analysis*, Master's Thesis, Milwaukee, Wisconsin, May 2004.

[22] SMARZEWSKI P., *Modelowanie statycznego zachowania niesprężystych belek żelbetowych wykonanych z betonu wysokiej wytrzymałości*, Monografie, Politechnika Lubelska, Lublin, 2011.

[23] Eggert G.M., Dawson P.R., Mathur K.K., *An Adaptive Descent Method for Nonlinear Viscoplas-ticity*, International Journal for Numerical Methods in Engineering, vol. 31, 1991, p. 1031-1054.

P. SMARZEWSKI

Rozwiązanie numeryczne belki żelbetowej metodą Newtona-Raphsona ze spadkiem adaptacyjnym

Streszczenie. W pracy przedstawiono rozwiązanie numeryczne belki żelbetowej. Modelowanie przeprowadzono z wykorzystaniem zasad Metody Elementów Skończonych (MES). W celu zweryfikowania modeli materiałowych: betonu i stali zbrojeniowej, porównano otrzymane wyniki obliczeń numerycznych metodą Newtona-Raphsona ze spadkiem adaptacyjnym, z wynikami doświadczalnymi. Symulacje mogą pomóc w obniżeniu kosztów badań doświadczalnych poprzez efektywniejsze planowanie eksperymentów. Możliwe jest rozwiązanie złożonych problemów zachowania konstrukcyjnych elementów żelbetowych w zakresie odkształceń liniowo-sprężystych i nieliniowych aż do zniszczenia.
Słowa kluczowe: mechanika konstrukcji betonowych, metoda elementów skończonych, belka żelbetowa, spadek adaptacyjny